Direct extraction of the mean particle size from a digital hologram

Loïc Denis, Corinne Fournier, Thierry Fournel, Christophe Ducottet,
Dominique Jeulin

Direct extraction of mean particle size from a digital hologram

Loïc Denis, Corinne Fournier, Thierry Fournel, Christophe Ducottet

Laboratoire Traitement du Signal et Instrumentation

UMR CNRS 5516

Bât. F, 10 rue Barrouin, 42000 Saint-Etienne, France

loic.denis@univ-st-etienne.fr

Dominique Jeulin

Centre de Morphologie Mathématique

Ecole des Mines de Paris

35 rue saint-Honoré, F-77300 Fontainebleau, France

Digital holography, consisting of both acquiring the hologram image in a digital camera and numerically reconstructing the information, offers new and faster ways to make the most of a hologram. We describe in this paper a new method to get the rough size of particles in an inline hologram. It relies on a property specific to interference patterns in Fresnel holograms: self-correlation of a hologram gives access to size information.

The proposed method is both simple and fast and gives results with acceptable precision. It suppresses all "numerical depth of focus" related problems when analysing large depth volumes.

1. Introduction

The potential of holography to measure particle size has been pointed out since its very beginnings.[1] The development of optical holography applications in fluid mechanics[2,3] proved the capability of holography to give access to both particle size and position in 3D.

Holography is a technique that allows a description of a 3D distribution of particles to be stored on a two dimension detector. Digital holography suppresses the wet chemical processing step and makes it possible to acquire and analyze volume objects within a short time, the limiting factor being the numerical processing speed. Many contributions have been brought over last past years on particle digital holography (see for example papers published in 4). On the one hand, efforts are put towards precise results through tridimensional image processing of the reconstructed volume. The objective is quality in this quest to reach holography's limit.[5,6,7] On the other hand, the need for fast processes adequate with inline monitoring or dynamic studies raises new challenges. Speed becomes primordial over precision in this class of applications. Three dimensional volume reconstruction and analysis are no longer feasible and information has to be directly extracted from the hologram. We describe in this paper a novel method corresponding to this latter approach. The aim of the method is to obtain the mean size of particles from an inline hologram. It is compared with a classical technique from the former approach.

Digital reconstruction of a hologram is achieved through numerical solving of the diffraction integral. Fresnel's transform has been shown[8] to be well adapted to the reconstruction of particle holograms. A focus plane located at a distance z_r from the recorded hologram I_H has a complex amplitude $\underline{A_{z_r}}$ given by:[8]

$$\underline{A_{z_r}} = I_H * \underline{h_{z_r}}$$

where $*$ stands for bidimensional convolution and $\underline{h_{z_r}}$ denotes Fresnel function with parameter z_r: $\underline{h_{z_r}}(x,y) = 1/(j\lambda z_r) \exp\left(j\pi(x^2+y^2)/(\lambda z_r)\right)$ (Fresnel function is underlined to emphasize its complex nature, j denotes the imaginary unit).

In the case of particle holograms, the analysis of the reconstructed volume can lead to

particle per particle size measurements.[9,6,10] Global estimation of the particles average size is however possible in a simpler and therefore faster method through direct analysis of the hologram. We describe this direct extraction method in the following section. The key step to get the size information is to compute the hologram self-correlation. The result of this operation is further analysed in section 3. Results on numerically generated and experimental holograms are given in section 4.

2. Principle of the method

We describe here how to extract a global size information from an in-line hologram of spherical opaque particles. In-line digital holography setup records the intensity of the incident coherent beam, diffracted when crossing the object and free propagated towards the digital sensor (see fig. 1). The reference wave and the object wave are not separate beams but a unique one which gives a good stability to the setup adapted to industrial application constraints. However the drawback of this experimental setup however is the restriction to low concentration particle volumes. Royer[11] qualifies inline particle holograms to be of good quality if the projected particles area is less than 1% of the hologram area.

We derive in this section the hologram intensity expression and show that its self-correlation carries the particle aperture self-correlation information. This information is connected with the particles size information.

2.A. *Approximated expression of the hologram intensity*

Let us derive a classical approximation for the hologram intensity expression.[12] An opaque spherical particle may be considered as a diffractive disk (whose aperture will be denoted ϑ_{r_i} with r_i the radius) located at the (x_i, y_i, z_i) position of the particle center. The diffracted unitary plane wave at the recording distance in Fresnel approximation is given by:[13]

$$\underline{A_z} = t_i * \underline{h_{z_i}}$$

$$= 1 - \vartheta_{r_i} * \underline{h_{z_i}} * \delta_{x_i, y_i}$$

where t_i represents the transmittance of the plane z_i and δ_{x_i,y_i} is Dirac's delta function located at point (x_i, y_i).

If we consider the incoming wave to remain quasi-plane for each particle, which is justified for low density holograms, the resulting diffracted wave in the recording plane becomes:

$$\underline{A_z} \approx 1 - \sum_{i=1}^{N} \vartheta_{r_i} * \underline{h_{z_i}} * \delta_{x_i,y_i} \tag{1}$$

Sensors only respond to intensity, related to the complex amplitude via the following relation: $I_H = |\underline{A_z}|^2$. The recorded hologram intensity can therefore be expanded as follows:

$$I_H = 1 - 2\sum_{i=1}^{N} \vartheta_{r_i} * \Re(\underline{h_{z_i}}) * \delta_{x_i,y_i} + \sum_{i=1}^{N}\sum_{j=1}^{N} \left(\vartheta_{r_i} * \underline{h_{z_i}} * \delta_{x_i,y_i} \right) \times \left(\vartheta_{r_j} * \underline{h_{-z_j}} * \delta_{x_j,y_j} \right).$$

where $\Re$ is used to denote the real part of a complex number.

The second term is predominant over the third one under the hypothesis of both small particles and low concentration holograms.[14] This last approximation results in the following "pattern-oriented" hologram intensity expression where each particle induces an interference pattern and where inter-particle interferences are neglected:

$$I_H \approx 1 - 2\sum_{i=1}^{N} \vartheta_{r_i} * \Re(\underline{h_{z_i}}) * \delta_{x_i,y_i}. \tag{2}$$

2.B. Hologram information coding

The interference pattern produced by a particle is characteristic of its position and size (see fig. 2). The pattern center indicates the transversal location (x_i, y_i) of the particle. The frequency modulation of the concentric rings carries the distance information (z_i) whereas their amplitude modulation depends on the distance to diameter ratio . Size measurements therefore seem to require digital reconstruction followed by distance estimation as a first step.

2.C. Self-correlation

As we shall underline later, self-correlation plays a key role to reach direct numerical extraction of size information in a hologram. Self-correlation is commonly used in the image

4

processing field to identify the size of different underlying structures in an image.[15] For instance, the relationship between the self-correlation of a binary image of spheres and their size distribution was studied in depth in the field of stereology.[16] It is therefore quite legitimate to apply this technique on our holograms as a potential direct size extraction method. It should however give us access to pattern sizes (see fig. 3(a)), proportional to $\lambda z_i/r_i$ ratio instead of the desired particle size. We show in this section that in the case of these very special patterns, self-correlation however gives the particle size (fig. 3(b)).

Let us recall a key property of Fresnel functions:[17] the *duality*, which may be written as: $\underline{h_z} \star \underline{h_z} = \delta$, using $\star$ as a symbol for (complex) correlation. The real part of Fresnel functions verify a weakened version: $\Re(\underline{h_z}) \star \Re(\underline{h_z}) = \frac{1}{2}(\delta + \Re(\underline{h_{2z}}))$. This implies that the self-correlation expression of the centered hologram $\tilde{I}_H$ can be expanded into three terms:

$$\tilde{I}_H \star \tilde{I}_H = 2 \sum_{i=1}^{N} \vartheta_{r_i} * \vartheta_{r_i} \tag{3a}$$

$$+ 2 \sum_{i=1}^{N} \vartheta_{r_i} * \vartheta_{r_i} * \Re(\underline{h_{2z_i}}) \tag{3b}$$

$$+ 4 \sum_{i=1}^{N} \sum_{\substack{j=1 \\ j \neq i}}^{N} \vartheta_{r_i} * \vartheta_{r_j} * \Re(\underline{h_{z_i}}) * \Re(\underline{h_{z_j}}) * \delta_{x_i - x_j, y_i - y_j} \tag{3c}$$

An example of such a self-correlation can be seen in figure 4 as a 3D surface representation. This representation emphasizes the breaking down into 3 terms: the central peak corresponds to term (3a), the concentric waves to term (3b) and the smaller peaks spread all over the surface to the final term (3c).

The first term (3a) is the sum of the self-correlation of each particle's aperture. It is directly connected with particle sizes. We name the second term (3b) "twin self-correlation" as it originates from holography's classical virtual images. The self-correlation operation, acting as a kind of self-restitution, gives rise to both the "objects" (i.e. particle aperture self-correlations) and their "twins" that seem located at a distance twice each particle recording distance. Finally, the third term (3c) arises from inter-particles correlations and therefore depends on the spatial distribution of the particles. Contrary to the first two, this last term is of anisotropic nature.

5

If we consider both (3b) and (3c) as noise, or perturbative terms, the centered hologram self-correlation unexpectedly depends only on the particle aperture self-correlations. The obtained self-correlation is that of an image with every particle in focus. The direct correlation of holograms has been studied previously by Poon and Kim and applied to 3D object matching[18] and 3D object location.[19] To the best of our knowledge, the object size information has never been connected with the hologram self-correlation before.

2.D.   Hologram processing chain

The relative importance of each term in equation 3 is investigated more deeply in section 3. Methods used to reduce the influence of the perturbative terms (3b) and (3c) are described there. We focus here on the hologram processing chain we suggest for direct particle size extraction (fig. 6(b)). This processing chain is compared with that of the classical approach (fig. 6(a)).

The centered hologram is analyzed through self-correlation calculation. Since useful information (3a) is isotropic, we can restrict ourselves to a 1D profile of the correlation. The size information is then directly extracted from this profile (see figure 6(b)). The processing chain is both simple and fast since the most heavy computing step is that of self-correlation which is done through two Fast Fourier Transforms. Let us note that as the required range for self-correlation is limited to its central part (the range width equals the particle diameter) direct estimation of the correlation (i.e. without Fourier transforms) could be faster in some cases.

The second step, namely 1D profile extraction, is achieved through a radial averaging operation. The final and last step consists in computing a best fitting line to get the rough mean size.

Classical particle size measurements using digital holography is achieved in four steps (fig. 6(a)), requiring quite heavy computing. The reconstruction step (first step in figure 6(a)) is the most computationally expensive. It requires at least 10 Fast Fourier Transform to reconstruct a volume slice around a particle depth position. In case of the study of large depth

volumes, 10 Fast Fourier Transform per particle are necessary. The reconstructed volume then has to be segmented (step 2) and labeled (step 3). Both these operations are applied on tridimensional images representing heavy memory loads. The final measurement step gives the size of each particle which leads to the granulometric distribution. This approach gives more complete and precise size information at a higher computing cost.

3. Relative importance of self-correlation components

We described in previous section 2.C the origin of each component of the centered hologram self-correlation. We focus in this section on their relative influence compared with particle aperture self-correlations (term (3a)).

The approximated expression for the diffracted wave amplitude given in equation 1 makes it possible to numerically generate realistic holograms. A hologram intensity distribution is obtained by taking the squared modulus of the computed complex amplitude. The phase information available in numerical simulations offers the possibility to illustrate the relative importance of each component of the centered hologram self-correlation. As an illustration, we generated numerically a hologram (see figure 7(a)) and computed its self-correlation profile (fig. 7(b)). This profile is the sum of different components drawn in figure 8: (a) particles aperture self-correlations, (b) "twin self-correlations" , (c) particles cross-correlations and (d) non linear terms.

3.A. Particle self-correlations

Term (3a) is the sum of each particle aperture self-correlation. For a disk of given radius r, the expression of its self-correlation can be derived analytically: $C_r(h) = 2r^2 \left(\arccos(\frac{h}{2r}) - \frac{h\sqrt{1-\frac{h^2}{(2r)^2}}}{2r} \right)$ for $h < 2r$ and $C_r(h) = 0$ for larger values of h. The graphical representation of C_r (fig. 5) is quite close to its tangent at the origin. The intersection of this tangent with the abscissa axis is proportional to r and therefore can be used to retrieve the diameter from the self-correlation profile.

The range $[0, 2r]$ of this term is short compared to the hologram size: the whole information

we will search for is located at small values of h (see fig. 8(a)). Since particles are isotropic, this term also is. In case of particles of different sizes in the hologram field, larger particles are more influential than smaller ones as their energy (i.e. area of their aperture) is more important. Moreover, intereference patterns that are partially lost outside the hologram boundaries tend to reduce the contribution of the corresponding particles.

3.B.   Twin self-correlations

Term (3b) is a set of concentric rings whose frequency modulation is roughly that of a Fresnel function with parameter $2\lambda\bar{z}$ ($\bar{z}$ denoting the average z distance of the particles). It is negligible in the range $[0, 2r]$ for large enough values of $\lambda\bar{z}$. It reaches indeed its maximum value close to the maximum of $\Re(h_{2z})$: for $h \approx \sqrt{\lambda z}$ which is well over $2r$. It's maximum value reduces in proportion to $1/z$.

This term is computed in figure 8(b) from the numerically generated complex amplitude $\underline{A_z}$ using the following relation: $\Re\left(\underline{\tilde{A}}_z \star \underline{\tilde{A}}_z^{\,*}\right) = \sum_{i=1}^{N} \vartheta_{r_i} * \vartheta_{r_i} * \Re(\underline{h_{2z_i}})$. In this example the maximal value of this term in the range $[0, 2r]$ is around 0.3% the maximum of term (3a).

3.C.   Particle cross-correlations

Term (3c) consists in peaks with the same spatial extent $2r$ as term (3a) but spread on the whole correlation image (see figure 4). At low densities of particles – compatible with holographic inline setup – this term is highly anisotropic. It is therefore strongly attenuated through a radial average. This term depends on the particles spatial distribution.

The curve drawn in figure 8(c) corresponds to both this term and the boundary effects. It is indeed computed as the difference between the self-correlation of a centered hologram generated using equation (2) and terms (3a) and (3b). Term (3a) has been obtained using the analytical expression given in section 3.A and therefore does not take into account boundary effects appearing when interference patterns go beyond the boundaries of the hologram.

The influence of this term in figure 8(c) is less than 1% the maximum of term (3a).

3.D. *Non linear terms*

Remaining terms come from the linear approximation made in equation 2. These terms might seem more problematic as they are not easily modeled and then suppressed. Moreover, they sum up at the origin of the correlation. Their influence for low concentrated holograms of relatively small particles however appears to be of limited weight: less than 1% in figure 8(d).

4. Results on numerical generated and experimental holograms

4.A. *Processing of numerically simulated holograms*

Since the perturbative terms listed in the previous paragraphs (b) to (d) are nearly negligible in our range of interest $[0, 2r]$, we will process in a first approach the centered hologram self-correlation as if it were formed only of term (3a). To increase robustness to noise, we will however not use the root of the correlation tangent at the origin (fig. 5) but the root of the best fitting line computed in a range coarsely corresponding to $[r/5, 3r/5]$. This range is chosen to minimize the influence of the perturbative terms. It is refined using the root found as an estimate for r. The correspondence between the root found and the actual particle diameter is set up during a calibration step. This step consists in comparing the root computed through self-correlation to the known calibrating size.

The experimental parameters used for the numerical simulation are described in figure 9(a). Spatial distributions of 10 particles have been randomly generated inside a volume with a large thickness: $50mm$. Each particle has got the same size for a given hologram.

Holograms of particles for 7 different sizes have been generated. For each defined size, 25 holograms corresponding to 25 independent realizations of the particles spatial distribution were generated leading to the study of 175 holograms.

A sample hologram is shown in figure 9(b). Even though every particle has the same size, the interference patterns vary from one particle to another because of the large depth of the studied volume (from $100mm$ to $150mm$). This effect is also pictured in the aforementioned figure 3.

Correlation profiles for sets of particles at each studied size ($70\mu m$ to $130\mu m$ by $10\mu m$

steps) are drawn in figure 9(c). The lowest curve corresponds to the smallest particle size: $70\mu m$ while the highest is bound to the maximum particle size: $130\mu m$. The linear dependence of profiles slopes on particle sizes is clearly visible.

Quantitative results are displayed in table 1. For each diameter appearing on the first line of the table, 25 holograms were generated. The absolute and relative errors were computed. Their averages over the 25 realisations are displayed in the second and third rows. A numerical calibration was carried out with a particle of $90\mu m$. The relative error remains small (less than 4%) over a wide range of diameters.

Numerical simulation points out that the method is valid when applied to realistic-looking holograms. The computed errors seem adequate with some real world applications.

4.B.   Hologram of a spray

We perform in this section a check of the self-correlation method on an experimental hologram. The setup is described in the next paragraph. The classical approach based on 3D analysis of the reconstructed planes is carried out as a reference measurement. Our new correlation based approach is then applied to the hologram and the obtained size is compared with that of the reference (classical) approach.

The studied object is a cloud of water droplets produced by a water spray (the velocity of the particles remained less than $10m/s$). The spray was lightened by a collimated beam (see inline setup in figure 1) produced by a YAG pulsed laser ($\lambda = 532nm$) whose pulse duration has been set to $7ns$. The hologram was therefore almost instantaneously recorded. The camera used has a dynamic range of 12 bits and its sensor is a 1280×1024 CCD matrix of $6.7\mu m$ width full-square pixels. The studied part of this hologram (830×744) is shown on figure 10(a).

The 3D particle localizing and diameter measurements have been done accordingly to the hologram processing chain depicted in figure 6(a) and presented in section 2.D. The droplets are located within a bounding volume of $60mm$ depth and the size particle ranges from $80\mu m$ to $110\mu m$ (see table 2 and figure 11 for a 3D reconstruction). The mean diameter of the ten

holographed particles is estimated at $84\mu m \pm 7\mu m$.

Direct extraction of the size information was achieved according to the self-correlation approach. The obtained correlation profile is drawn in figure 10(b). The whole hologram analysis using this approach takes less than $2s$ to compute on an average PC. The size found from the correlation profile is $91\mu m$. This size appears to be over-estimated, which is easily explained by the size variations from the smallest to the biggest particle. As previously underlined in section 3.A, larger particles have a higher weight than smaller ones in the correlation profile. The size found using the correlation approach then is in accordance with the results obtained through the classical approach.

5. Conclusion

Classical particle size measurement from a digital hologram require the reconstruction of more than 10 images per particle. This leads to heavy computing unsuitable with inline monitoring. In this study we have described and applied experimentally a direct and fast method to extract the mean particle diameter from an inline hologram. The principle of the method can be seen as an original application of the classical self correlation technique used in image processing to extract the mean size of objects. The key of the method is the duality property of Fresnel function which allows a sort of "self reconstruction" when computing the self correlation. Each interference pattern is indeed convolved with the recording function stored in its concentric rings.

This approach differs from classical ones in that it does not require to reconstruct the object but extracts the wanted information directly from the hologram.

The advantages of this method are the simplicity and the stability of the optical setup, the large depth of field of holography and the speed of the image processing (compared with the classical approach). It should be well adapted to a large class of industrial applications. This method can be used as a first step for a refined analysis of the reconstructed volume. Techniques such as those based on correlation require the knowledge of pattern sizes to access sub-pixel particle locating.[20,9] The described method gives quickly this necessary size

information.

Let us notice that this method can be extended to objects with other shapes than disks and then allows to obtain rough measurements of sizes and the main orientation in the set of objects. Studies carried in the field of stereology also describe how to extract more information from a correlation profile, namely how to estimate parameters of a given distribution function of sizes.

References

1. B. J. Thompson. A new method of measuring particle size by diffraction techniques. *Japanese Journal of Applied Physics*, 4(1):302–307, 1965.

2. C. S. Vikram. *Particle field holography*. Cambridge University Press, 1992.

3. K.D. Hinsch. Holographic particle image velocimetry. *Measurement Science and Technology*, 13:R61–R72, 2002.

4. K. D. Hinsch and S. F. Herrmann. *Special Feature : Holographic Particle Image Velocimetry*, volume 15 of *Measurement Science & Technology*. IOP, United Kingdom, 2004.

5. J. Müller, V. Kebbel, and W. Jüptner. Characterization of spatial particle distributions in a spray-forming process using digital holography. *Measurement Science & Technology*, 15(4):706–710, 2004.

6. G. Pan and H. Meng. Digital holography of particle fields: reconstruction by use of complex amplitude. *Applied Optics*, 42:827–833, 2003. R21.

7. C. Fournier, C. Ducottet, and T. Fournel. Digital in-line holography: influence of the reconstruction function on the axial profile of a reconstructed particle image. *Measurement Science & Technology*, 15:686, 2004.

8. T.M. Kreis, M. Adams, and W. Juptner. Methods of digital holography : A comparison. In Christophe Gorecki, editor, *SPIE97*, volume 3098, pages 224–233, Munich, Germany, 1997.

9. S. Murata and N. Yasuda. Potential of digital holography in particle measurement. *Optics and Laser Technology*, 32(7 8):567–574, 2000.

10. M. Malek, S. Coëtmellec, D. Allano, and D. Lebrun. Formulation of in-line holography process by a linear shift invariant system: application to the measurement of fiber diameter. *Optics communications*, 223:263–271, 2003.

11. H. Royer. An application of high-speed microholography: the metrology of fogs. *Nouv. Rev. Opt*, 5:87–93, 1974.

12. L. Onural and P.D. Scott. Digital decoding of in-line holograms. *Optical Engineering*, 26(11):1124–1132, 1987. Corinne, Holographic Particle Diagnostics Vikram.

13. J.W. Goodman. *Introduction to Fourier Optics*. Mc Graw-Hill, 1996.

14. C. Buraga-Lefebvre, S. Coëtmellec, D. Lebrun, and C. Özkul. Application of wavelet transform to hologram analysis: three-dimensional location of particles. *Optics and Lasers in Engineering*, 33(6):409–421, 2000.

15. J. Serra. *Image analysis and mathematical morphology*. Academic Press, London, 1982.

16. D. Jeulin. Random models for the morphological analysis of powders. *Journal of Microscopy*, 172(Part 1):13–21, 1993.

17. M. Liebling, T. Blu, and M. Unser. Fresnelets : New multiresolution wavelet bases for digital holography. *IEEE Transactions on image processing*, 12(1):29–43, 2003.

18. T.-C. Poon and T. Kim. Optical Image Recognition of Three-Dimensional Objects. *Appl. Opt.* , 38:370–381, January 1999.

19. T. Kim and T.-C. Poon. Three-dimensional matching by use of phase-only holographic information and the Wigner distribution. *Optical Society of America Journal A*, 17:2520–2528, December 2000.

20. C. Fournier, C. Barat, C. Ducottet, and T. Fournel. Digital holography applied to piv : hologram reconstruction and selection of a cloud of particles in the reconstructed volume. In *Pacific Symposium on Flow Visualization and Image Processing*, Chamonix, France, 2003.

Table 1. Results of the correlation method on numerically generated holograms. In the first row are displayed the correct diameters used to generate the holograms. The second and third row give the errors made when retrieving the diameters.

Diameter (μm)	70	80	90	100	110	120	130
Absolute error* (μm)	1.6	1.7	0.8	1.0	1.7	3.2	4.8
Relative error* (%)	2.3	2.1	0.9	1.0	1.5	2.7	3.7

*Displayed errors are average errors on computed diameters from 25 numerically generated holograms

Table 2. Positions and sizes of the particles in figure 10(a) experimental hologram. Displayed data has been obtained via analysis of the reconstructed volume using classical techniques.

Particle		1	2	3	4	5	6	7	8	9	10
	x (mm)	3.326	2.287	4.460	2.061	3.658	4.694	4.023	3.610	0.737	1.884
Position	y (mm)	3.972	4.754	4.046	3.738	2.955	3.692	1.073	1.403	3.428	0.809
	z (mm)	40.0	45.8	47.5	49.5	65.0	69.6	69.8	81.0	95.4	101.3
Diameter (μm)		79	91	96	65	79	71	79	81	89	108

List of Figures

Fig. 1. In-line digital holography setup.

Fig. 2. Hologram information coding: a line profile (in black stroke), Fresnel radial frequency modulation function (dash point line) and the diffraction envelope (dashed line).

| $z = 400r$ | $z = 800r$ | $z = 1000r$ | $z = 1200r$ | $z = 1400r$ |
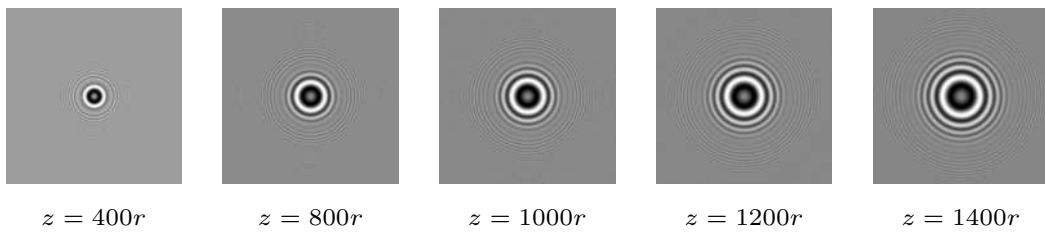
(a) Diffraction pattern produced by a particle located at an increasing distance z
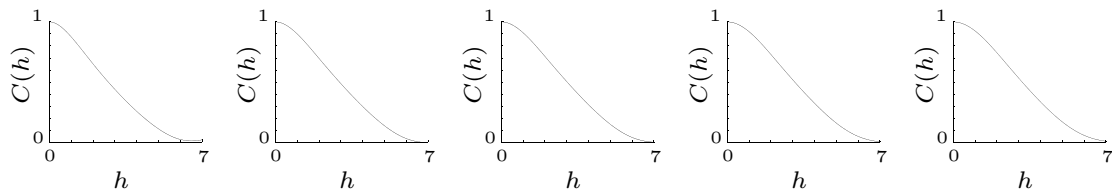
(b) Corresponding correlation profiles

Fig. 3. Patterns of a particle with constant radius r for different recording distance z and their associated self-correlation profile.
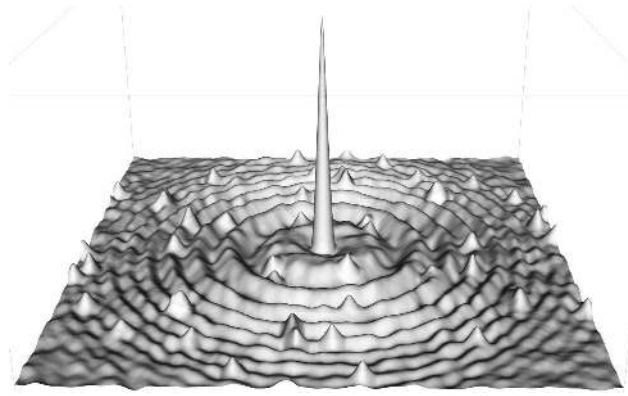
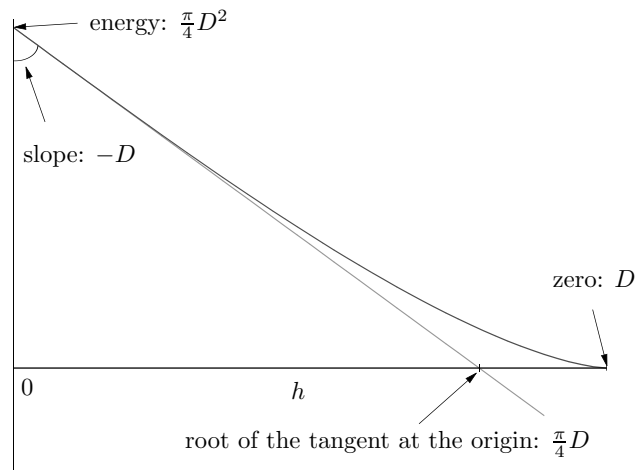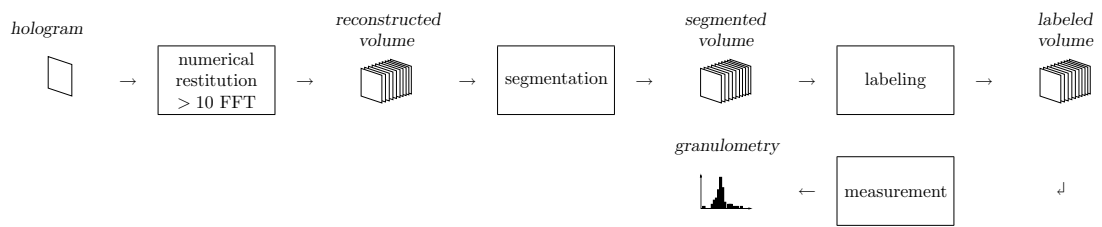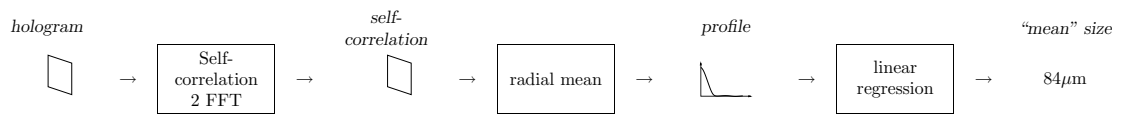Fig. 4. Centered hologram self-correlation (numerical simulation).

energy: $\frac{\pi}{4}D^2$

slope: $-D$

zero: D

0

h

root of the tangent at the origin: $\frac{\pi}{4}D$

Fig. 5. Self-correlation of a disk.

hologram → numerical restitution > 10 FFT → reconstructed volume → segmentation → segmented volume → labeling → labeled volume

granulometry ← measurement ↵

(a) Classical hologram processing chain for size measurements

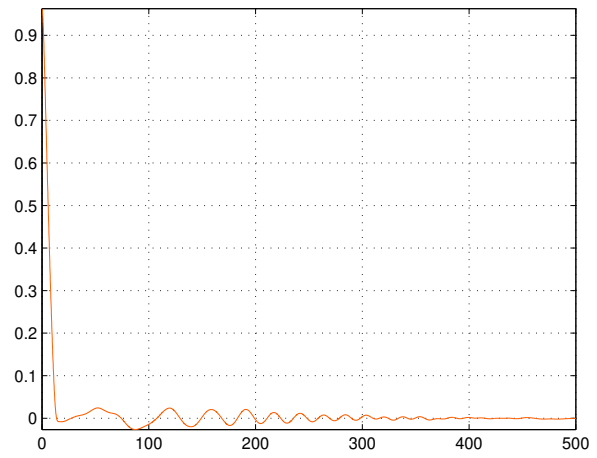hologram → Self-correlation 2 FFT → self-correlation → radial mean → profile → linear regression → "mean" size 84μm

(b) The proposed direct particle size extraction scheme

Fig. 6. Hologram processing chain.
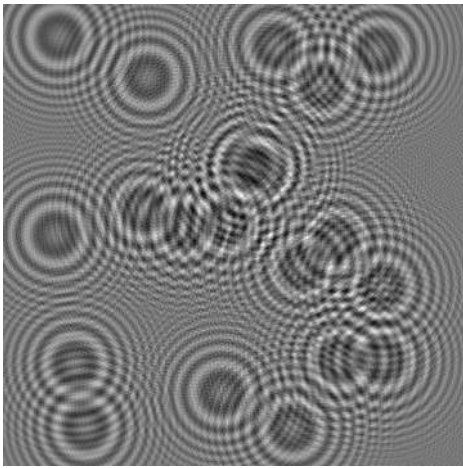
(a) Numerically generated hologram

(b) Corresponding centered self-correlation

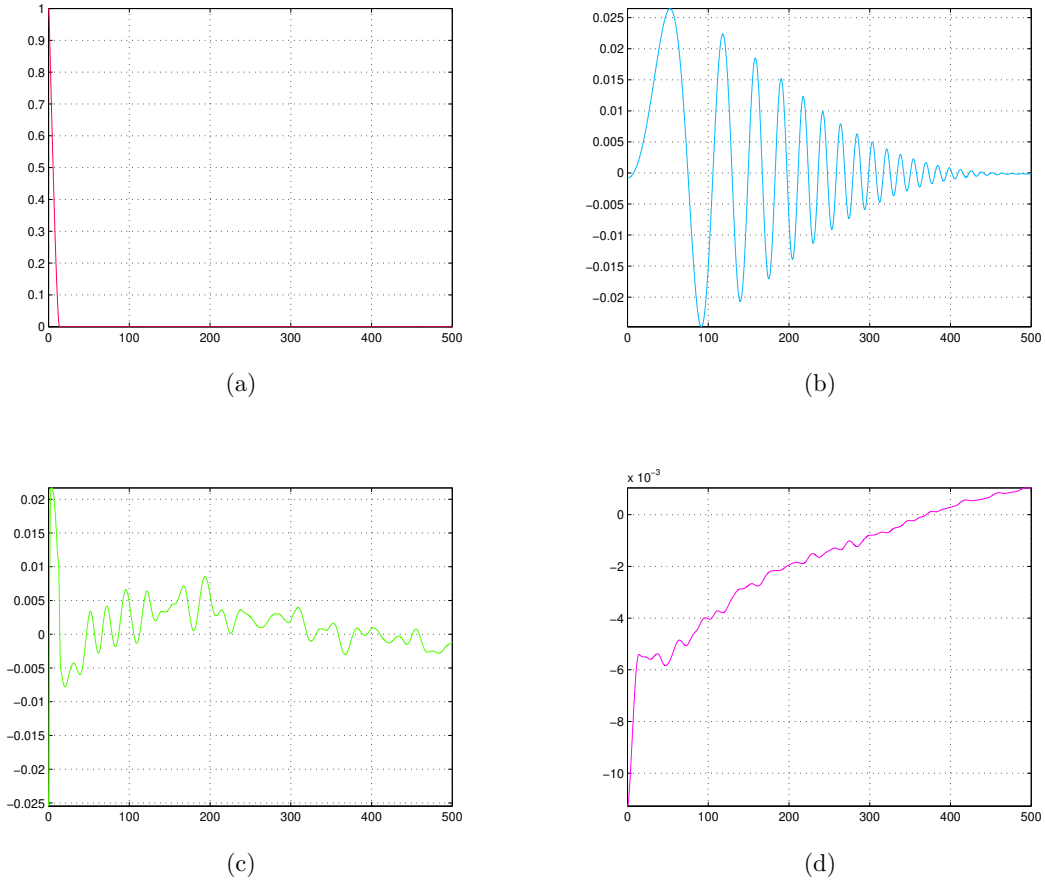Fig. 7. A hologram and its self-correlation profile.

Fig. 8. Breaking down of fig. 7(b) correlation profile into the 4 constituent terms: (a) particle apertures self-correlations term, (b) "twin self-correlations term, (c) cross-correlations term and (d) non linear terms.
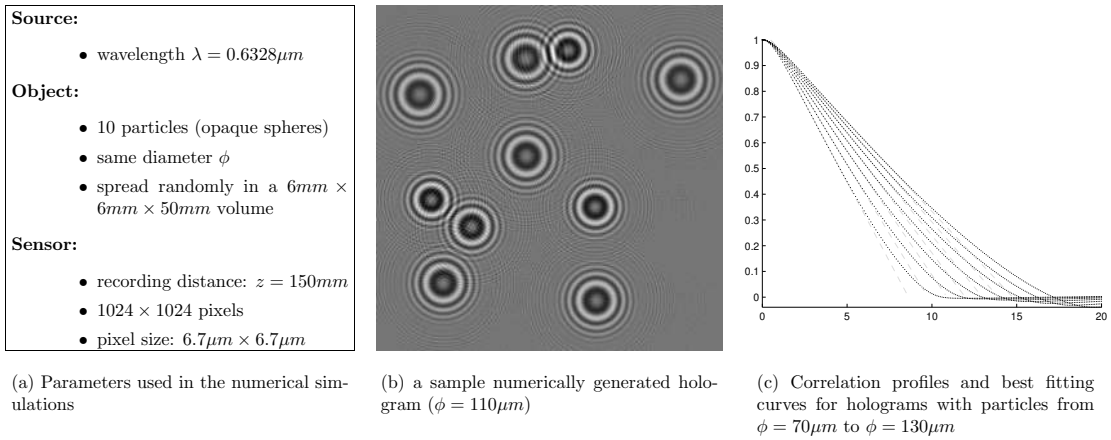
(a) Parameters used in the numerical simulations

Source:
- wavelength $\lambda = 0.6328\mu m$

Object:
- 10 particles (opaque spheres)
- same diameter ϕ
- spread randomly in a $6mm \times 6mm \times 50mm$ volume

Sensor:
- recording distance: $z = 150mm$
- 1024×1024 pixels
- pixel size: $6.7\mu m \times 6.7\mu m$

(b) a sample numerically generated hologram ($\phi = 110\mu m$)

(c) Correlation profiles and best fitting curves for holograms with particles from $\phi = 70\mu m$ to $\phi = 130\mu m$
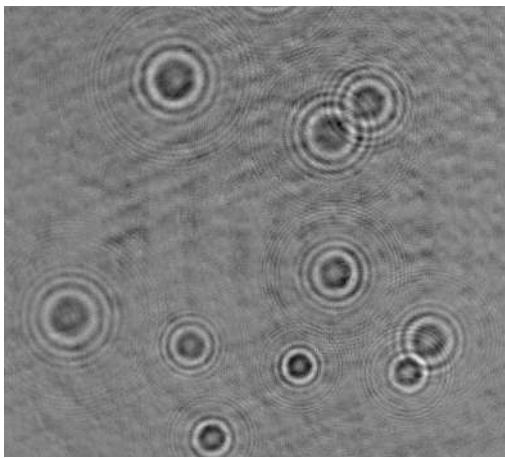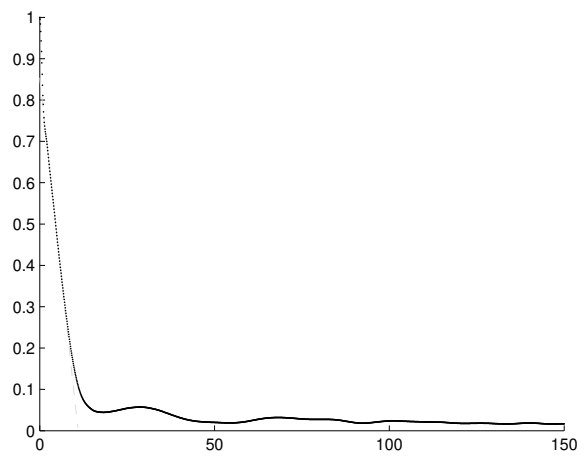
Fig. 9. Application of the size extraction method on numerically generated holograms.

(a) Experimental digital hologram of water droplets in the air

(b) Correlation profile computed on hologram (a)
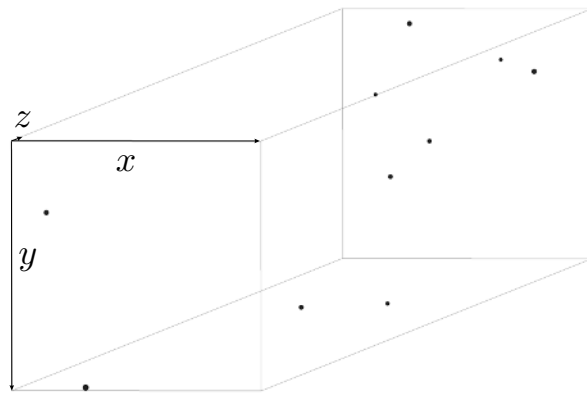
Fig. 10. Experimental result on a hologram of a water spray.

Fig. 11. Reconstructed volume from the experimental hologram of figure 10.